VIII International Conference on Computational Methods for Coupled Problems in Science and Engineering
COUPLED PROBLEMS 2019
E. Oñate, M. Papadrakakis and B. Schrefler (Eds)

FLUID STRUCTURE INTERACTION MODELLING ON FLAPPING WINGS

D. Risseeuw*, B. W. Van Oudheusden*, A. H. Van Zuylen* and G. Chourdakis†

* Department of Aerospace Engineering
Delft University of Technology
P.O. Box 5058, 2600GB, Delft, the Netherlands
e-mail: derekrisseeuw@gmail.com, a.h.vanzuijlen, b.w.vanoudheusden@tudelft.nl, web page: https://www.tudelft.nl/

† Department of Computer Science
Technical University of Munich
Boltzmannstraße 3, Garching, Germany
e-mail: chourdak@in.tum.de, web page: https://www5.in.tum.de

Key words: Computational Fluid Dynamics, Fluid Structure Interaction, FSI, Open-Source, Flapping Wings

Abstract. Flapping wings display complex flows which can be used to generate large lift forces. Flexibility in wings is widely used by natural flyers to increase the aerodynamic performance. The influence of wing flexibility on the flow can be computed using numerical analysis with Fluid Structure Interaction (FSI).

The influence of inertial, elastic and aerodynamic forces is quantified using a 2D wing. A sinusoidal flapping motion is imposed on the leading edge of the vertical wing. The inertial force on the wing dominates for high mass ratios and the wing deflection is rather independent of the flow. For a low mass ratio, the wing deformation scales with the increasing elasticity. The maximum lift and lowest drag were found for the wing with large flexibility and low mass so the passive deformation by aerodynamic forces creates a favourable shape for lift production.

Flexible translating and revolving wings at an angle of attack of 45 degrees show that chordwise flexibility decreases both lift and drag, however the lift over drag ratio is increased. The flow around both wings forms a coherent structure with a Root Vortex (RV), Tip Vortex (TV), Leading Edge Vortex (LEV) and Trailing Edge Vortex (TEV). The LEV on the revolving wing is stable for approximately up to half the span because vorticity is transported outward in the vortex core. The flowfield and LEV breakdown are consistent with experimental data of the same wing. The translating wing builds up circulation but the LEV detaches quickly near the centre of the wing. Chordwise bending reduces the angle of attack which decreases the distance to the core of the shed LEVs.

1 INTRODUCTION

Over the past years increased interest in Micro Air Vehicles (MAVs) has lead to an increase in research towards flapping wing aerodynamics. This research is often based on natural flyers as these display remarkable capabilities in force production, manoeuvrability and efficiency. Currently, these capabilities are unmatched by man-made flyers. The aerodynamic phenomena found on flapping wing are different from the classic airfoil theory that is used at higher Reynolds numbers. Unsteady phenomena play a large role in the force production by flapping wings. The Wagner effect, added mass effect, clap and fling effect, Kramer effect, wake capture effect, tip vortex contribution and a stable LEV. The latter effect was first recognised in 1996 and is often the most prominent feature for lift generation in flapping wing aerodynamics [10]. It is seen on wings moving at a high angle of attack which feature dynamic stall [20]. A vortex is formed over the leading edge which can remain stably attacked to the wing surface and creates a low pressure area inherent to the vortex with a large suction force on the wing. The suction force acts perpendicular to the wing surface and is dominant in lift production. The high suction force leads to a maximum in the lift coefficient for 45° angle of attack [17, 22, 18].

The motion of flapping wings is determined by an acceleration phase and a phase of rectilinear motion. Both translating and revolving wings at high angles of attack are capable of developing a LEV at the acceleration phase, but only for revolving wings the LEV can remain stably attached to the wing surface [15]. For translating wings a vortex streak is formed which resembles the von Kármán vortex street behind a cylinder. Early research postulated that the LEV stability in revolving wings was caused by outboard vorticity transport [10]. Subsequent researches evaluate the influence of the various apparent rotational effects on the LEV, and reach the conclusion that mainly the Coriolis force is responsible for the stability of the LEV [15, 13, 12]. The relative influence of the Coriolis force is related to the degree of translating versus rotating motion, expressed in the Rossby number. The rotational effects scale inversely with the Rossby number on the wing, and the LEV stability is deteriorates for higher Rossby numbers.

Apart from a different flapping motions, natural flyers exhibit flexible wings. Birds and bats actively deform their wings, while most insects rely on passive wing deformation [21]. Experimental research showed that the application of flexibility on a simple revolving wing leads to smaller lift but decreases the drag likewise [30]. Numerical research on 2D and 3D flapping wings showed that the wing efficiency for a given angle of attack can be increased by the application of flexible wings. The dynamic behaviour of the wing is categorised by the mass and frequency ratio, which determine the relative importance of the inertial, elastic and aerodynamic force on the wing. Flapping wing with a low mass ratio reach the largest lift over drag (L/D) for a frequency ratio near $FR = 1/3$ [27, 8, 16]. Heavier wings create an advanced pitching motion.

More recently, experiments towards the influence of flexibility on flapping wings was performed using tomographic PIV [26]. In this work a revolving wing was tested for three

wings with a varying elasticity. The lift and drag decreased for the added flexibility, but an increase in L/D ratio was noted. The flowfield showed similar structures with more coherency with increasing flexibility. Furthermore, the LEV of the flexible cases was more compact and showed higher levels of vorticity transport through the LEV core. Breakdown of the LEV is seen for all three wings around midspan after the wing revolved for approximately 40°.

Numerical modelling of the wing using a FSI method can be used to gain more insight in the fundamental interaction that takes place between the structure and the fluid. Several commercial methods exist for the modelling of FSI coupled simulations, however, on the open-source side a smaller variety is available. The most used open source CFD code, `openFOAM` does not include standard methods of creating a FSI simulation [1]. Recent progress by on a generic OpenFOAM adapter has opened the door for a new approach [7]. Coupling of the simulation is performed using the multi-physics coupling library `preCICE` [24]. The adapter was extended to support Fluid structure interaction modelling [19]. The method was validated along the Cylinder with a Flap benchmarking case [23]. In this paper the influence of flexibility in flapping wings is investigated using the newly developed FSI method. The following section treats the influence of flexibility on 2D flapping wing, where the influence of the wing mass and elasticity on the force coefficients is derived.

2 2D Flapping wing

In this section a simple hovering flapping wing in a 2D domain is considered, at the low Reynolds number of 150 [29]. The mass and stiffness of the wing are varied to change the relative importance of the aerodynamic, elastic and inertial forces which act on the wing. The structure for this case shows large, nonlinear deformations, therefore the case is solved in an implicit FSI simulation using the newly developed FSI method [19].

2.1 Model description

The flow around the wing is characterised by several non-dimensional numbers which can be obtained by combining the structure and fluid parameters. Figure 1 shows the wing with the kinematic parameters and with the surrounding mesh. The chord (c) and thickness (h) influence both the fluid and the structure side. The angle of attack is defined with respect to the horizontal direction x.

The wing kinematics are purely defined by the translation x_0 and angle of attack α of the wing at the leading edge. In the current set-up no phase differences between the translation and pitching of the wing are considered. The wing kinematics are determined by the following equations:

$$x_0(t) = \frac{A_0}{2}\cos(2\pi f t), \qquad \alpha(t) = \alpha_0 + \beta\sin(2\pi f t). \tag{1}$$

Following from the wing movement the non-dimensional time can be defined: $\tau = t/T$,

with T the period of the flapping motion: $T = 1/f$. The non-dimensional numbers are the Reynolds number, non-dimensional stroke amplitude, mass and frequency ratio:

$$Re = \frac{\pi A_0 f c}{\nu_f}, \qquad A^* = \frac{A_0}{c}, \tag{2}$$

$$m^* = \frac{\rho_s h}{\rho_f c}, \qquad FR^* = \frac{f}{f_n}. \tag{3}$$

where f_n is the frequency of the first bending eigenmode of the wing. The frequency ratio (FR) is a measure for the flexibility of the wing with respect to the fluid forces and is used to define the relative importance of elastic and inertial forces. Previous research has shown that there is an optimum in the frequency ratio such that the wing has the highest efficiency [27, 16, 8]. The mass ratio (m^*) defines the ratio between the aerodynamic forces and the inertial force. For a simple flapping wing with no active pitching the drag increases for higher mass ratios [16]. The forces generated by the airflow typically bend the wing into a shape with a lowered angle of attack, reducing the frontal area and thus the drag. The parameters used to set up the simulation are given in table 1. The relation between the fluid and structural component are determined using the expressions in equation 4

$$\rho_s = \frac{m^* \rho_f c}{h} \qquad E = \frac{12\rho_s}{h^2}\left(\frac{c}{k_n}\right)^4 \left(\frac{2\pi f}{FR}\right)^2, \tag{4}$$

where k_n is a constant for a given bending eigenfrequency.

Table 1: Set-up for the flexible flapping wing

Parameter	Value
c [m]	$1 \cdot 10^{-2}$
h [m]	$5 \cdot 10^{-4}$
ν_f [$\mathrm{m^2\,s^{-1}}$]	$5 \cdot 10^{-5}$
ρ_f [$\mathrm{kg\,m^{-3}}$]	10
f [$\mathrm{s^{-1}}$]	1.910

Table 2: Structural parameters for the flexible wings

m^* [-]	ρ_f [$\mathrm{kg\,m^{-3}}$]	E [$\mathrm{kg\,m^{-1}s^{-2}}$]		
		$FR = 1/6$	$FR = 1/4$	$FR = 1/3$
1	200	$3.295{\cdot}10^4$	$1.465{\cdot}10^4$	$8.240{\cdot}10^3$
5	1,000	$1.647{\cdot}10^5$	$7.320{\cdot}10^4$	$4.117{\cdot}10^4$
25	5,000	$8.235{\cdot}10^5$	$3.660{\cdot}10^5$	$2.059{\cdot}10^5$

The flexible definition of parameters easily allows for the choice of different settings. The mass ratio can be increased to increase the relative effect of inertial over aerodynamic forces. Three different mass ratios are tested as shown in table 2. In flapping wing analogy, the lowest mass ratio is comparable with a dragonfly wing, the $m^* = 5$ wing is close to a moths wing [9]. For the highest mass ratio the wing deformation is largely determined by the inertial forces [16].

2.2 Mesh sensitivity study

For the mesh sensitivity study a rigid wing is selected. $A_0 = 2.5c$ and $\beta = \pi/8$ in equation 1 define the sweeping and rotation of the wing. A small pitching angle is used to assert some asymmetry in vertical direction to the flowfield and to generate a finite average lift. An O-grid is shaped around the wing and extruded for 40 chord lengths to form a circular domain. A large domain is required to avoid large recirculation of shed vortices which create chaotic behaviour. A free inflow/outflow and zero pressure is applied on the outer boundary. The mesh surrounding the wing is shown in figure 1 for the coarsest grid.

Under the sweeping and rotational motion the mesh is deformed by solving the laplacian equation for the mesh displacement. To limit deformation and preserve the mesh quality the leading and trailing edge were rounded. The shape of the leading edge is of relative low importance for the overall flowfield, so the round-off is not expected to have a serious impact on the flow simulation [25]. Furthermore, the mesh cells are grown perpendicular with respect to the wing surface. It was found that this reduced the chance of large skewness or even cell collapse.

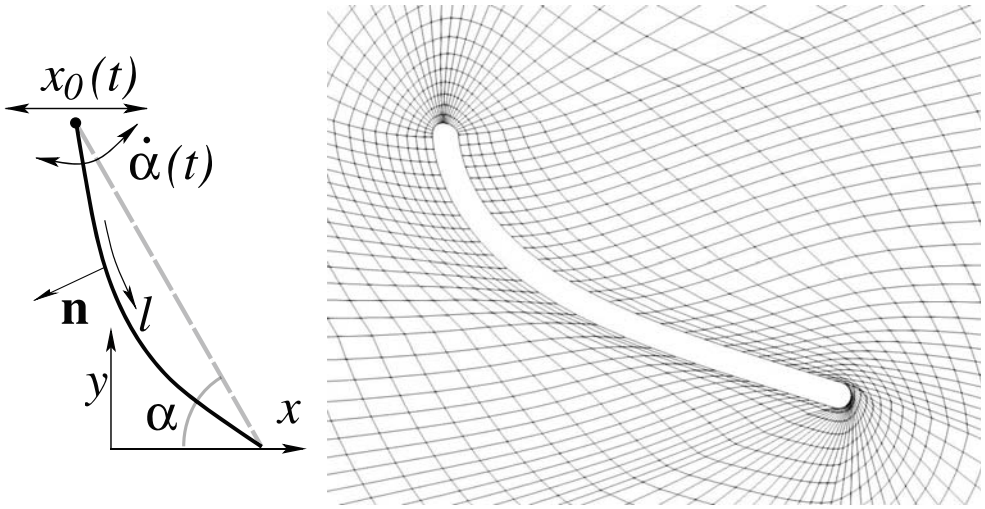

Figure 1: The flapping wing (left) definition of the motion [16]. (right) The mesh at critical deformation that shows the coarse O-grid is shaped around the wing. The motion is defined at the leading edge (top) of the wing.

The force coefficients are evaluated for three meshes of increasing refinement. The coarse mesh has 4,968 elements. The normal and fine mesh feature respectively 19,440 and 77,760 elements. The wing surface is refined with respectively 54, 108 and 216 cells, which leads to an average mesh spacing of approximately $0.02c$ for the coarsest mesh. This is comparable to the mesh spacing used in similar research [29].

Figure 2 shows the phase-averaged lift and drag over the wing for 6 flapping periods.

The drag is defined as the force opposite to the direction of travel, so the drag vector changes direction during supination and pronation. The range in which the lift and drag occurred over this range of periods is shaded. From $\tau = 0$ to $\tau = 0.5$ the wing is in upstroke. While the wing kinematics imposed to the wing movement are completely symmetric, the lift and drag show very different graphs for the up- and downstroke. This means that the flow is determined to a large extend by the shed vortices of the previous motion.

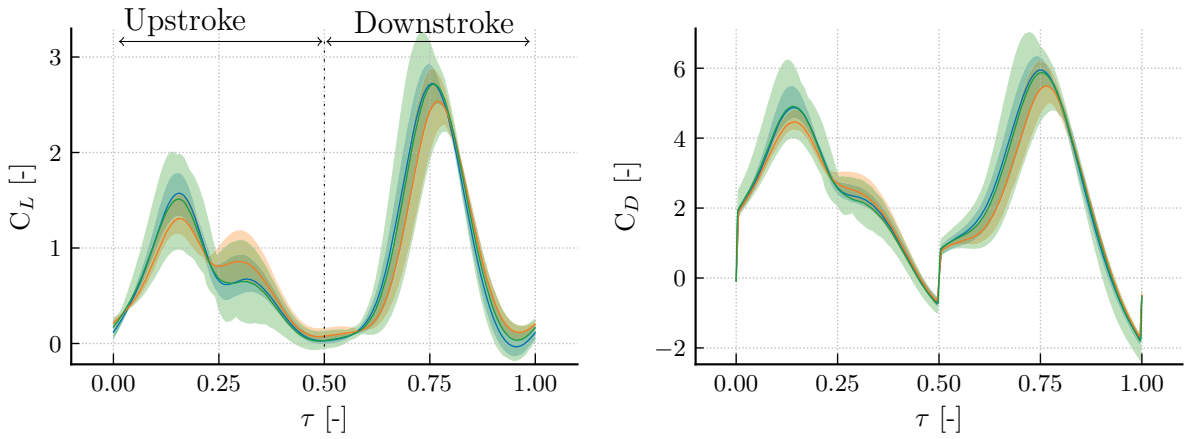

Figure 2: (left) Lift and (right) drag coefficients for one flapping period. The line represents the average value over 6 periods, and the shaded area represents the range perceived during these periods. — Coarse, — Normal and — Fine mesh.

The total average value for the lift and drag (shown in table 3) shows good correlation for the average lift and drag.

Taking the finest mesh as the most accurate solution, both the coarse mesh and the normal mesh fall within the range of the average force value plus or minus the average maximum deviation. Over the range of the motions over 6 periods, it is clear that the average lift and drag of the coarse mesh fall within the possible values for the normal mesh and fine mesh.

Figure 3: Average lift and drag coefficient and the average maximum deviation over 6 periods

Refinement	C_l [-]	ΔC_l [-]	C_d [-]	ΔC_d [-]
Coarse	0.82	0.10	2.46	0.22
Normal	0.79	0.11	2.29	0.23
Fine	0.83	0.26	2.47	0.59

The mesh deformation method described earlier performs significantly better with coarser meshes. It is less prone to collapse under large rotation and deformation. Since the behaviour of the coarse mesh shows good correlation with the fine mesh, it is selected to investigate the effect of different mass and frequency ratios.

2.3 Results

Flexibility is added to the wing according to the parameters given in table 2. Furthermore a rigid wing with the same kinematics is tested to obtain the limiting case of $FR = 0$. The wing kinematics are defined by a pure sweeping motion: $A_0 = 2.5c$ and $\beta = 0$. This entails that the wing can only obtain an angle of attack by structural bending. The effect of the mass ratio on the tip displacement and force coefficients is shown in figure 4 for four wings: Rigid, and $m^* = [1, 5, 25]$ with a frequency ratio of $FR = 1/3$. The first eigenfrequency is noted for all three wings as the oscillation with a value three times the flapping frequency.

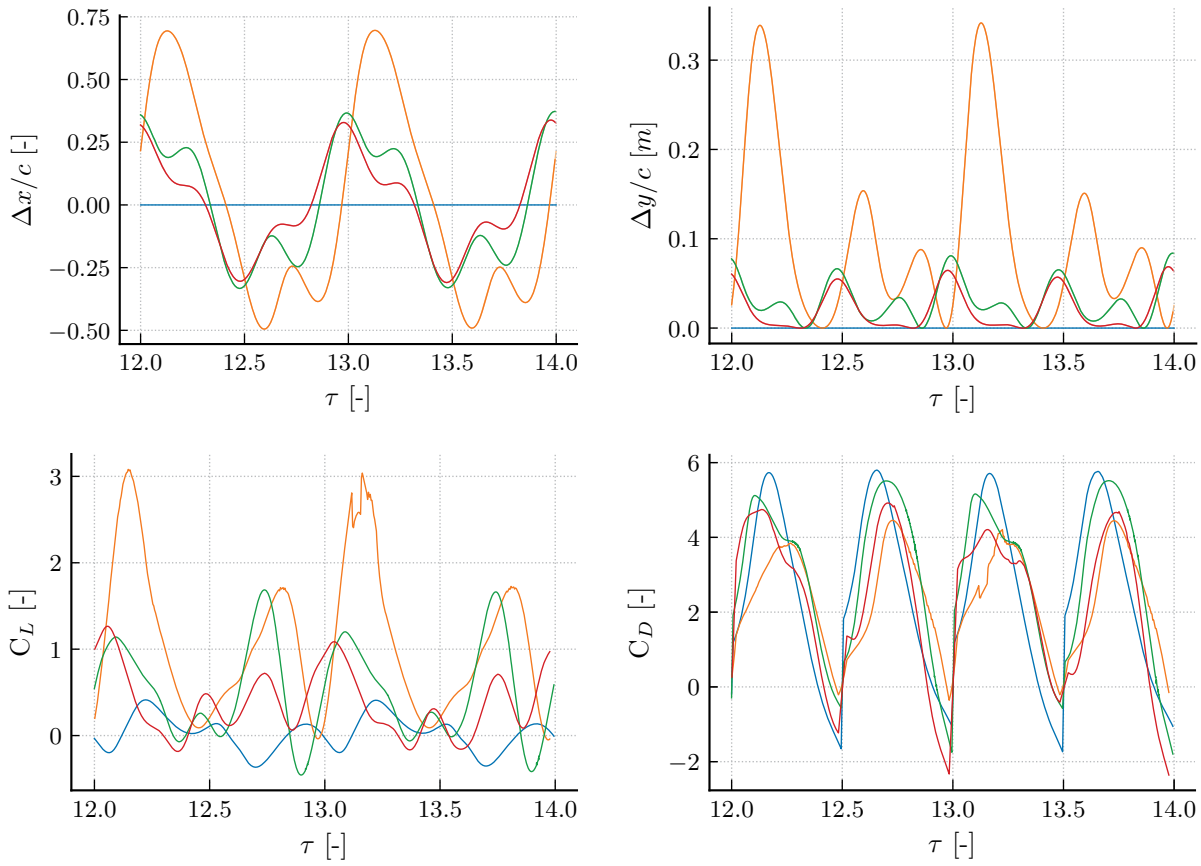

Figure 4: Influence of the mass ratio m^* on the (top) tail x- and y displacement and (bottom) lift and drag coefficient over two flapping periods. —Rigid, —$m^* = 1$, —$m^* = 5$, —$m^* = 25$

The tail deflection with respect to the rigid position shows that the wing with the smallest mass ratio has a phase delay with respect to the two heavy wings. Furthermore the deflection of the wing is much larger, with a maximum horizontal deflection of approx-

imately 0.7 chordlength. The delay and larger amplitude of the deflection means that the light wing creates a lower angle of attack during both the up- and downstroke. In both these strokes a large portion of lift is created, whereas the drag is comparable or smaller to the other wings. Large asymmetry is caused because the shedding behaviour between both strokes is different, as will be treated later.

Small differences can be seen between the $m^* = 5$ and $m^* = 25$ wing but these are far less pronounced than the differences with the lightest wing. For both these wings the deflection is nearly symmetrical between up- and downstroke, while the aerodynamic forces are not. As soon as the wing decelerates during midstroke, the deflection in x-direction changes sign. During both the middle part of the up- and downstroke the $m^* = 5$ wing maintains a higher deflection, which is caused by a LEV which stays closely attached to the wing. The low pressure favours a larger lift and drag creation during this phase of high translational velocity. During the latter part of the stroke a small portion of thrust is created by the wing because of the advanced rotation.

In figure 4 the lift and drag profile for the wing with $m^* = 1$ shows irregular behaviour at the point of large displacement. The discontinuous force coefficients are caused by large fluctuations in the pressure field between timesteps. This represents the limits of the current mesh deformation method.

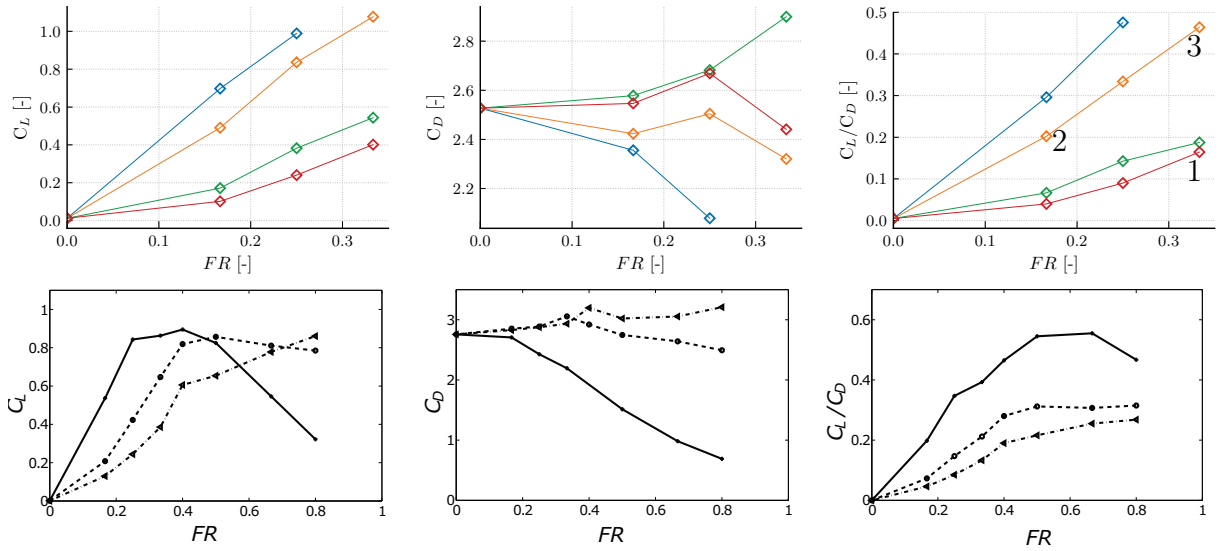

Figure 5: Average (left) lift and (middle) drag coeffient, and (right) lift over drag ratio for different mass ratios. (top) FSI simulations with —$m^* = 0.5$, —$m^* = 1$, —$m^* = 5$ and —$m^* = 25$. (bottom) the reference case with —$m^* = 1$, - - -$m^* = 5$ and ·-·-$m^* = 25$ [16]. Note the scale difference on the x-axis between the top and bottom figures. For both the FSI simulations and the reference data the forces are averaged over 15 periods. The flowfield of points 1, 2 and 3 is shown in figure 6

The effect of a higher stiffness by changing the frequency ratio (FR) causes the elastic effect to dominate the wing movement in the latter part of the stroke. During the acceleration part of the stroke, the wing is deflected by the wings' mass (inertial force). The aerodynamic forces can help to maintain this deflection during the latter part of the stoke and prolong a lower angle of attack. This effect is most pronounced for the most flexible wings. A larger deflection causes a lower angle of attack and decreases the frontal area. The drag history shows a clear that the drag is reduced for a large portion of the stroke for more flexible wings. However, the advanced rotation by the stiffer wings create a small portion of thrust, as also seen for the rigid wing. This lacks for the most flexible wings.

Figure 5 displays the average lift and drag coefficient, and lift over drag ratio for all the tested wings over 15 flapping periods. A wing with an even lower mass ratio of $m^* = 0.5$ is incorporated for two additional mass ratios, which indicates the limit of the mesh deformation method. Furthermore, reference data is shown on the bottom row for same wing geometry and kinematics, where a wing was tested up to frequency ratios of 0.8 [16].

For the tested range of flapping frequencies any flexibility increases the lift over the wing. The wing bending creates a lower angle of attack which points the residual fore more towards the lift direction. Furthermore, a clear relation can be distinguished between the mass ratio and the lift. Lower mass ratios lead to a higher lift for this range of the frequency ratio. This result is also seen for the reference data. The relative higher importance of the aerodynamic forces with respect to the inertial forces helps in maintaining a lower angle of attack throughout the latter part of the stroke. The highest lift coefficient is obtained for the $m^* = 1$ and $FR = 1/3$ wing with a value of $C_L = 1.076$. It appears that the delayed rotation of the wing for low mass ratios helps in decreasing the drag on the wing by reducing its frontal area. The advanced rotation by the heavier wings initially increases the drag. The peak for the $m^* = 5$ wing at a frequency ratio of $FR = 1/3$ is featured in both the reference data and the simulated data. This point is interesting since it shows a different behaviour for the wings with $m^* = [5, 25]$ and $FR = 1/3$. Up to this point the lift and drag of these two wings were very similar.

For this frequency range a straightforward relation is seen between the lift to drag ratio. A more flexible wing leads to higher ratios. Also the lightest wings create higher lift over drag ratios by means of a high lift creation. This is in good agreement the reference data which shows the same trend for this range of frequency ratios [16]. In figure 6 the vorticity flowfield around three wings is shown for one flapping motion. The vorticity is normalised according to: $\omega^* = \omega \frac{U}{c}$. The left column indicates the wing in which the inertial force is dominant: $m^* = 25$, $FR = 1/3$, named hereby wing 1. The middle figure shows the wing 2 with dominance of the elastic forces: $m^* = 1$, $FR = 1/6$. The latter column shows the wing 3 for which the three forces are more balanced. This wing features the highest lift and lift over drag ratio in the tested range.

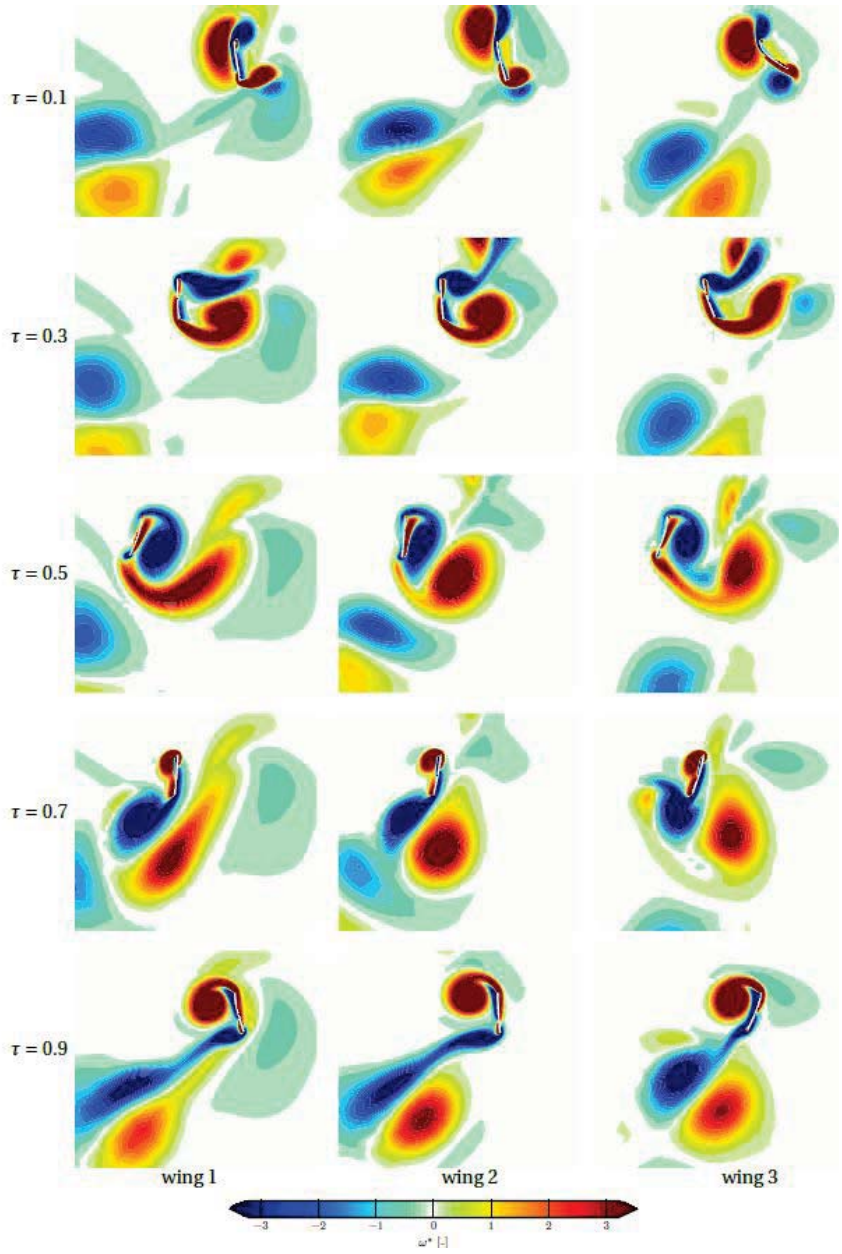

Figure 6: Non-dimensional in-plane vorticity (left) $m^* = 25$ and $FR = 1/3$. (middle) $m^* = 1$ and $FR = 1/6$. (right) $m^* = 1$ and $FR = 1/3$. A representative period is taken and the time instance is scaled to the time.

All three cases shows a similar shedding of the vortices. In the beginning of the period ($\tau = 0.1$), the LEV of the previous stroke remains close to the wing surface and is convected both above and below the wing after stroke reversal. The wake capturing causes rapid build-up of vorticity on the leading edge, but the newly formed LEV can not stay attached closely to the wing ($\tau = 0.3$). At stroke reversal ($\tau = 0.5$), the LEV catches up with the wing and it is shed under the wing and forms counter rotating vortex pair with the previous TEV. The shed vortex pair has a larger downward component for wing 3 compared to the other wings. This indicates that it is more efficient in inducing downward momentum in the flow, while the other wings create a larger horizontal momentum.

Without the wake capturing, the formation of a new LEV takes longer, and around ($\tau = 0.7$) a compact core can be seen around the LE which has grown to a large LEV with significant force contribution near the end of stroke.

The effect of the mass ratio is most evident by the phase of the flapping motion. Neglecting the amplitude of the deflection, the shape of the wing 3 is often similar to that of wing 1 in for $\tau - 0.2$, which indicates a phase delay of $1/5^{th}$ of a period.

Comparing the effect of the wing frequency ratio shows that the vortical structure of the flows are very similar. Also the wing displacement shows smaller effect of the phase delay. Only at $\tau = 0.9$ wing 2 is clearly already near 90° angle of attack, while wing 3 still has a much lower value. The main difference in flowfield is caused by the lower angles of attack of the flexible wing. This helps pointing the resulting force in the direction of the lift vector, while reducing the drag at the same time. For wing 1 the upstroke has a larger deflection and is responsible for the major part of lift production. This effect is much less pronounced for wing 2, since its shape is more determined by elastic forces.

3 CONCLUSIONS

The section above treats the influence of different degrees of stiffness and mass of a flapping 2D wing. The newly developed FSI method is able to capture well the relative importance of the various forces that occur on the flapping wing [19]. A simple translation motion is prescribed without any pitching. The stiffness and mass of the wing determine the relative effect of the inertial and elastic forces and can be related to the aerodynamic forces by defining the frequency ratio (FR) and mass ratio (m^*).

A large mass ratio renders the fluid forces insignificant due to high inertial forces. The wing deformation is determined by the wing kinematics and hardly by the influence of the flowfield. As soon as the wing starts to decelerate during midstroke the wing deflection is reversed shortly after. A light wing shows a deflection which causes lowered angle of attack during almost the entire stroke because the aerodynamic forces help to sustain the angle of attack. The advanced rotation of the higher mass ratio wings is not beneficial for the production of lift. For the investigated range of flapping frequencies, a lower mass ratio always leads to a higher lift and lift over drag ratio. The influence of the frequency ratio is more predictable. The deflection is lower for stiffer wings which creates lower lift and higher drag. The more rigid wings show a slight advance in pitching behaviour.

The horizontal flapping motion creates an asymmetric flowfield between the up- and downstroke which was present for every combination of the mass ratio and frequency for the tested cases. The wings with a relative large influence from the aerodynamic forces to be are influenced by the asymmetry in the flowfield and show a difference in deflection between the up- and downstroke. Especially for the wing with $m^* = 1$ and $FR = 1/3$ this difference is pronounced. Wings dominated by either elastic or inertial forces are less affected by the flowfield and show more symmetric deflection of the trailing edge.

The results regarding the influence of the mass and frequency ratio obtained in this section are in good agreement with comparable research [16]. Therefore the FSI module is able to simulate the relative importance of the various forces in flapping wing aerodynamics.

References

[1] Openfoam and the openfoam foundation. `https://openfoam.org/`, 2018.

[2] J. D. Anderson. *Fundamentals of Aerodynamics*. McGraw-Hill series in aeronautical and aerospace engineering. McGraw-Hill Education, 5th edition, 2011.

[3] J. M. Birch and M. H. Dickinson. Spanwise flow and the attachment of the leading-edge vortex on insect wings. *Nature*, 412(6848):729–733, Aug. 2001.

[4] J. M. Birch, W. B. Dickson, and M. H. Dickinson. Force production and flow structure of the leading edge vortex on flapping wings at high and low reynolds numbers. *J. Exp. Biol.*, 207(7):1063, Feb. 2004.

[5] D. S. Blom, A. H. van Zuijlen, and H. Bijl. Multi-level acceleration with manifold mapping of strongly coupled partitioned fluid-structure interaction. *Computer Methods in Applied Mechanics and Engineering*, 296(Supplement C):211–231, Nov. 2015.

[6] J. M. Chen and Y.-C. Fang. Strouhal numbers of inclined flat plates. *Journal of Wind Engineering and Industrial Aerodynamics*, 61(2):99–112, July 1996.

[7] G. Chourdakis. precice-adapter for the cfd code openfoam. `https://github.com/precice/openfoam-adapter`, 2017.

[8] H. Dai, H. Luo, and J. F. Doyle. Dynamic pitching of an elastic rectangular wing in hovering motion. *Journal of Fluid Mechanics*, 693:473–499, 2012.

[9] T. L. Daniel and S. A. Combes. Flexible wings and fins: Bending by inertial or fluid-dynamic forces? *Integrative and Comparative Biology*, 42(5):1044–1049, 2002.

[10] C. P. Ellington, C. van den Berg, A. P. Willmott, and A. L. R. Thomas. Leading-edge vortices in insect flight. *Nature*, 384(6610):626–630, Dec. 1996.

[11] D. Garmann and M. R. Visbal. A numerical study of hovering wings undergoing revolving or translating motions. In *31st AIAA Applied Aerodynamics Conference*, Fluid Dynamics and Co-located Conferences. American Institute of Aeronautics and Astronautics, June 2013.

[12] T. Jardin. Coriolis effect and the attachment of the leading edge vortex. *Journal of Fluid Mechanics*, 820:312–340, 2017.

[13] T. Jardin and L. David. Coriolis effects enhance lift on revolving wings. *Phys. Rev. E*, 91(3):031001, Mar. 2015.

[14] T. Jardin, A. Farcy, and L. David. Three-dimensional effects in hovering flapping flight. *Journal of Fluid Mechanics*, 702:102–125, 2012.

[15] D. Lentink and M. H. Dickinson. Rotational accelerations stabilize leading edge vortices on revolving fly wings. *J. Exp. Biol.*, 212(16):2705, July 2009.

[16] H. Luo, B. Yin, H. Dai, and J. Doyle. A 3D computational study of the flow-structure interaction in flapping flight. In *48th AIAA Aerospace Sciences Meeting Including the New Horizons Forum and Aerospace Exposition*, Aerospace Sciences Meetings. American Institute of Aeronautics and Astronautics, Jan. 2010.

[17] M. Percin and B. W. van Oudheusden. Three-dimensional flow structures and unsteady forces on pitching and surging revolving flat plates. *Experiments in Fluids*, 56(2):47, Feb. 2015.

[18] N. Phillips and K. Knowles. Effect of flapping kinematics on the mean lift of an insect-like flapping wing. *Proceedings of the Institution of Mechanical Engineers, Part G: Journal of Aerospace Engineering*, 225(7):723–736, July 2011.

[19] D. Risseeuw. Fluid structure interaction modelling of flapping wings. mathesis, Delft University of Technology, Jan. 2019.

[20] S. P. Sane. The aerodynamics of insect flight. *J. Exp. Biol.*, 206(23):4191, Oct. 2003.

[21] W. Shyy, H. Aono, and C.-k. Kang. *An Introduction to Flapping Wing Aerodynamics*. Cambridge University Press, New York, UNITED STATES, 2013.

[22] P. Trizila, C.-K. Kang, H. Aono, W. Shyy, and M. Visbal. Low-Reynolds-number aerodynamics of a flapping rigid flat plate. *AIAA Journal*, 49(4):806–823, Apr. 2011.

[23] S. Turek and J. Hron. Proposal for numerical benchmarking of fluid-structure interaction between an elastic object and laminar incompressible flow. In *Fluid-Structure Interaction: Modelling, Simulation, Optimisation*, pages 371–385. Springer Berlin Heidelberg, Berlin, Heidelberg, 2006.

[24] B. Uekermann. Precice. `https://github.com/precice`, 2017.

[25] J. R. Usherwood and C. P. Ellington. The aerodynamics of revolving wings i. model hawkmoth wings. *J. Exp. Biol.*, 205(11):1547, June 2002.

[26] R. van de Meerendonk. Three-dimensional flow and load characteristics of flexible revolving wings at low Reynolds number. mathesis, Delft University of Technology, June 2016.

[27] M. Vanella, T. Fitzgerald, S. Preidikman, E. Balaras, and B. Balachandran. Influence of flexibility on the aerodynamic performance of a hovering wing. *Journal of Experimental Biology*, 212(1):95–105, 2008.

[28] F. White. *Viscous Fluid Flow*. McGraw-Hill Education, 2005.

[29] B. Yin and H. Luo. Effect of wing inertia on hovering performance of flexible flapping wings. *Physics of Fluids*, 22(11):111902, Nov. 2010.

[30] L. Zhao, Q. Huang, X. Deng, and S. P. Sane. Aerodynamic effects of flexibility in flapping wings. *Journal of The Royal Society Interface*, 7(44):485–497, 2010.